Journal of The Electrochemical Society, **158** (10) A1155-A1159 (2011)
0013-4651/2011/158(10)/A1155/5/$28.00 © The Electrochemical Society

Particle Interaction and Aggregation in Cathode Material of Li-Ion Batteries: A Numerical Study

M. Zhu,[a,*] J. Park,[a] and A. M. Sastry[a,b,c,z]

[a]*Department of Mechanical Engineering,* [b]*Department of Material Science Engineering, and* [c]*Department of Biomedical Engineering, University of Michigan, Ann Arbor, Michigan 48109, USA*

Aggregation between additive particles and active particles in the electrode material of batteries strongly affects their interfacial impedance and power performance. This paper proposes a three dimensional model to simulate the aggregation process of carbon black (CB) and $LiMn_2O_4$ active material (AM) particles within a liquid medium (PVDF polymer dissolved in NMP solvent). Brownian dynamics is employed in the simulation and the resulting aggregates are characterized by the number of CB particles connected to the percolated cluster of AM. The effects of the particle size, CB/AM mass ratio and temperature are investigated. It is found that a larger AM particle size and larger CB/AM mass ratios each contributes positively to the percentage of CB attachment. However, with increasing temperature this percentage increases in cases where AM particles have a diameter of 1 μm but decreases for AM particles whose diameter is 0.5 μm.
 [DOI: 10.1149/1.3625286]

Manuscript submitted April 12, 2011; revised manuscript received June 21, 2011. Published August 16, 2011.

Extensive efforts have been made to lower the internal resistance and increase the energy density of Li-ion batteries due to the demanding performance requirements for electric vehicle (EV) and hybrid electric vehicle (HEV) applications. However, the energy storage capacity of a Li-ion cell is provided by active material (e.g. $Li_xMn_2O_4$) that has very low conductivity.[1,2] This low conductivity limits battery power performance. Conductive additives [e.g. carbon black (CB)] of dimension orders of magnitude smaller are typically added to improve the conductivity of electrodes. A polymer binder [e.g. polyvinylidene difluoride (PVDF), polytetrafluoroethylene (PTFE)] (Refs. 3–6) is used to combine electrode materials into an integrated system and provide mechanical integrity. However, these additives, which vary in scale (Fig. 1), increase the total mass of the battery.

Figure 1 shows a schematic of the cathode system, indicating active material particles and conductive additive particles. The active material particles are usually secondary particles consisting of primary particles and have a size ranging from less than 1 to 100 μm. The primary active material particles have a size in the order of 1 μm. The size of conductive additive particles is in nanometer scale.[7] Several forces and parameters (such as viscous forces, Brownian forces, temperature, conductive additive to active material mass ratio and particle size distribution) have been thought to be responsible for the morphology of electrode material.[8–10] Experimental studies have previously been conducted on the morphology of cathode materials.[8–11] It has been observed that the active material, conductive additive and polymeric binder form different self-assembled characteristic structures according to the composition of the cathode. For example, it has been found that a higher polymer binder to conductive additive ratio facilitates the contact of the active material and the conductive additive, helping forming a conductive network.[2,12] The morphology of the self-assembled structure in cathodes also plays an important role in the structural integrity. Local fracture has been observed in cathode materials and has been implicated as a capacity fade mechanism causing loss of electric contact in the secondary particles.[13–15] At the aggregate level, fractures occurring within or between secondary particles may disrupt connectivity, causing loss of conductivity in the cathode.

In order to optimize the composition of cathodes to improve capacity and power density, the appropriate balance of materials needs to be determined. It has been reported that interfacial impedance dominates cell impedance, and while the additives and binders improve conductivity and power performance by forming self-assembled characteristic structures,[11,16] they represent a parasitic mass, thus reducing the gravimetric energy and density. An optimal balance between conductive additives and polymeric binders is also required. While a higher PVDF content reduces self-attraction of AB particles, improving cathode capacity at high C-rates; however the electrode conductivity increases and then decreases with increasing AB/PVDF ratio. Based upon these observations, it has been suggested that the electrical and ionic conductivities of the cell strongly depend on the final structure of electrode materials, and that structure is directly affected by the interaction of the constituents during electrode fabrication. Accurate reproduction of aggregates via simulation can help predict the impact of fracture on the conductivity in the aggregate level.

Previous work has used Brownian dynamics simulations to model colloidal aggregation of monodisperse systems.[17–19] Binary systems have also been modeled using Brownian dynamics simulations. For example, in the work of Cerbelaud et al.,[20] the heteroaggregation of AlO particles (~200 nm) and SiO nanoparticles (~12.5 nm) was simulated, and it has been reported that a suspension of AlO particles can be destabilized by a small amount of SiO particles, leading to the formation of aggregates.

Despite the above-mentioned experimental observations and the potential benefits from understanding and optimizing the aggregation process of the electrode material structure through simulation, due to the complexity of electrode material interaction.

A robust algorithm to simulate this interaction process and identify the key energetic drivers and aggregates characteristics has not yet been developed. In our present study our objectives are as follows: (1) develop a simulation algorithm to model the self-assembly process during electrode fabrication; (2) characterize the morphology of the self-assembled structures; (3) identify the effect of particle size, mass ratio and temperature on the morphology of the self-assembled structures.

Methods

Brownian dynamic simulation.—We performed a Brownian dynamic simulation to model the aggregation of CB and AM particles. The trajectory of the particles is governed by the Langevian equation

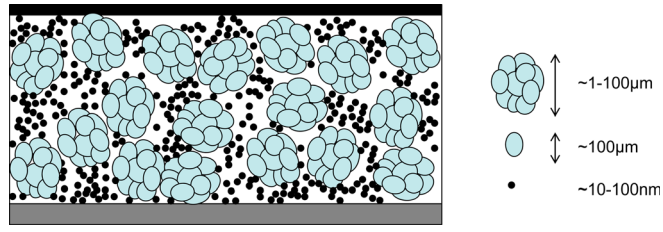

Figure 1. (Color online) Illustration of cathode materials.

* Electrochemical Society Student Member.
z E-mail: amsastry@umich.edu

$$m_i \frac{d\mathbf{v}_i(t)}{dt} = -\zeta_i \mathbf{v}_i(t) + \sum_j \mathbf{F}_{ij}\{\mathbf{r}_{ij}(t)\} + \mathbf{\Gamma}_i(t) \quad [1]$$

where m_i is the mass of the i-th particle; $\mathbf{v}_i$ is the velocity of the i-th particle; $\mathbf{F}_{ij}$ is the force exerted on the i-th particle by the j-th particle; $\mathbf{r}_{ij}$ is the position vector from the j-th particle to the i-th particle; $\zeta_i = 6\pi\eta a_i$ is the friction coefficient that depends on the solvent viscosity η, simulating Stokes' friction, which represents the only hydrodynamic interaction considered in this study. $\mathbf{\Gamma}_i(t)$ represents the interaction between CB and/or AM particles with surrounding PVDF-NMP solution molecules, obeying the following statistical properties

$$\langle \mathbf{\Gamma}_i(t) \rangle = 0, \text{and} \langle \mathbf{\Gamma}_i(t)\mathbf{\Gamma}_j(t') \rangle = C\delta(t-t')\delta_{ij} \quad [2]$$

where $C = 2k_B T\zeta_i$ with k_B the Boltzmann constant and T the temperature. The integration schemes are given by Eqs. (3) and (4),[20] and time step size $\delta t = 4 \times 10^{-10}$ s

$$\mathbf{v}_i(t+\delta t) = \mathbf{v}_i(t) + \frac{\sqrt{2k_B T\zeta_i}}{m_i}(\delta t)^{1/2}\mathbf{Y}_i + \frac{1}{m_i}\left(-\zeta_i \mathbf{v}_i(t) + \sum_j \mathbf{F}_{ij}\{r_{ij}(t)\}\right)\delta t \quad [3]$$

$$\mathbf{r}_i(t+\delta t) = \mathbf{r}_i(t) + \mathbf{v}_i(t)\delta t \quad [4]$$

Note that $\frac{\sqrt{2k_B T\zeta_i}}{m_i}(\delta t)^{1/2}\mathbf{Y}_i$ is the random Brownian force term given by stochastic calculus. $\mathbf{Y}_i$ follows Gaussian distribution.

The DLVO (named after Derjaguin and Landau, Verwey and Overbeek) theory is employed[21] and the interaction between particles is viewed as the sum of two contributions: (1) attraction due to van der Waals forces U_{ij}^{vdW} and (2) electrostatic double layer interaction U_{ij}^{el} due to surface charges of the particles

$$U_{ij}^{DLVO} = U_{ij}^{vdW} + U_{ij}^{el} \quad [5]$$

The van der Waals contribution is represented as

$$U_{ij}^{vdW}(r_{ij}) = -\frac{A_{ij}}{6}\left[\frac{2a_i a_j}{r_{ij}^2 - (a_i + a_j)^2} + \frac{2a_i a_j}{r_{ij}^2 - (a_i - a_j)^2} + \ln\left(\frac{r_{ij}^2 - (a_i + a_j)^2}{r_{ij}^2 - (a_i - a_j)^2}\right)\right] \quad [6]$$

where a_i and a_j denotes the radius of particle i and j; A_{ij} is the Hamaker constant that depends on the polarizability of particles i and j and of the solvent.

The electrostatic contribution is represented as

$$U_{ij}^{el}(r_{ij}) = \pi\varepsilon\frac{a_i a_j}{a_i + a_j}\left(\psi_i^2 + \psi_j^2\right) \times \left[\frac{2\psi_i\psi_j}{\psi_i^2 + \psi_j^2}\ln\left(\frac{1 + e^{-\kappa h_{ij}}}{1 - e^{-\kappa h_{ij}}}\right) + \ln\left(1 - e^{-\kappa h_{ij}}\right)\right] \quad [7]$$

where $\varepsilon = \varepsilon_0\varepsilon_r$ is the dielectric constant of the solvent, ε_r is the relative dielectric constant and ε_0 is permittivity of the vacuum; ψ_i is the surface potential of particle i, $h_{ij} = r_{ij} - (a_i + a_j)$ is the surface-to-surface separation distance, and κ is the inverse Debye screening length 1×10^9 m^{-1} used in this simulation.

Simulation parameters.—We model the formation of the electrode structure, with manganese oxide as the active material (AM), CB as the conductive additive, and PVDF as the polymeric binder. The CB and AM are modeled as spherical particles. CB particles are simulated with a diameter of 60 nm, assuming they start from a very low level of agglomeration prior to the mixing process, and AM particles are simulated with a diameter of 0.5 or 1 μm in two different cases. PVDF binder is dissolved in an Anhydrous *N*-methylpyrrolidone (NMP) solution, forming a homogenous viscous medium.

The parameters of the constituents we used in this simulation can be found in Table I. The Hamaker constant of CB is given as 2.53×10^{-19} J.[22] The surface energy of NMP $\gamma_n = 0.04$ J/m^2 (Ref. 23) is used to calculate the Hamaker constant of NMP using equation $A = 24\pi\gamma_n D_o^2$,[22,24] and the Hamaker constant is found to be 8.21×10^{-20} J. The Hamaker constant between manganese oxide and Si_3N_4 in aqueous solution is 2.4×10^{-19}J (Ref. 25) and the Hamaker constant for water is 3.7×10^{-20} J.[26,27] The Hamaker constant of Si_3N_4 is given as 1.74×10^{-19} J.[28] The Hamaker constant of manganese oxide is then calculated from Eq. (8) to be 1.59×10^{-18} J.

$$A_{132} = \left(\sqrt{A_{11}} - \sqrt{A_{33}}\right)\left(\sqrt{A_{22}} - \sqrt{A_{33}}\right) \quad [8]$$

where A_{132} is the Hamaker constant between manganese oxide and Si_3N_4 in aqueous solution, A_{11}, A_{22} and A_{33} are the Hamaker constants for manganese oxide, Si_3N_4 and water respectively.

From Eq. (8), we calculated the Hamaker constant in NMP for CB-CB, manganese oxide-manganese oxide, and CB-manganese oxide, which are 4.69×10^{-20}, 9.5×10^{-19}, and 2.11×10^{-19} J, respectively.

The zeta potentials for the particles are -50 mV for CB (Ref. 29) and -30 mV for manganese oxide.[30] In our simulation, we take the zeta potential as the surface potential of CB and manganese oxide particles. NMP has a relative dielectric constant 32.0 (Ref. 31) and viscosity 1.67 mPa $*$ s.

CB and AM particles are initiated at random positions in this PVDF-NMP medium, simulating the initially homogenized system. The Brownian dynamic simulation[20,32] is then employed, and CB and AM particles are allowed to form aggregates in the PVDF-NMP medium until a stable structure is established.

The CB and AM particles are both simulated as spheres with densities of 2 g/cm^2 and 4 g/cm^2 respectively. 60 nm is used as the diameter for CB; in the simulations we varied the diameters of AM particles from 0.5 to 1.0 μm. The mass ratio for CB and AM is 1:23 and 1:11. The volume fraction of the total solid phase (CB and AM) in the simulation domain is 50%. In this work, 10 AM particles are simulated inside the domain with period boundary condition. The size of the simulation domain and the number of CB particles are calculated from the solid volume fraction and mass ratio of CB/AM. The number of CB particles is 629, 1315, and 5032 respectively for the cases with AM particle size 0.5 and 1.0 μm. Table II shows the parameter matrix that we explored in this work.

Figure 2 shows the normalized potential energy plotted against the normalized separation distance (surface distance) between different particles (in the case where the AM particle diameter equals 0.5 μm). From the monotonies of these curves we conclude that despite the repulsive electrostatic interactions between particles, the

Table I. Parameters associated to the electrode materials.

Material	Diameter (μm)	Density (g/cm^3)	Hamaker constant (J)	Relative dielectric constant	Zeta potential (mV)
CB	0.06	2.0	2.53e-19	—	−50
MnOx	0.5–1.0	4.0	1.59e-18	—	−30
NMP	—	—	8.21e-20	32.2	—

Table II. System parameters.

Mass ratio (CB:AM)	AM size (μm)	Temperature (K)
4:92 (%)	1.0	298
		308
		328
	0.5	298
		308
		328
8:88 (%)	0.5	298
		308
		328

overall forces are mainly attractive due to the contribution of the van der Waals interaction. We set up the potential cut-off distance at the points where interaction forces are negligible. The potential cut-off distance (from center to center) is 1.8 times the diameter of a single CB particle for CB-CB interaction, 1.2 times the diameter of a single AM particle for AM-AM interaction, and 0.6 times the diameter of a single AM particle for CB-AM interaction. A Verlet neighbor list with a radius of 2.2 times the cut-off distance was created as illustrated in Fig. 2d. The list was updated once the displacement of any particle was greater than half of this radius. At short range, the magnitude of the attractive force increased toward infinity, which is not realistic and in our numerical simulation would lead to particle overlapping. To avoid overlapping, the DLVO force curve was cut off at a short separation distance (1% the diameter of a CB particle for CB-CB interaction; 1% the diameter of an AM particle for AM-AM interaction; and 0.1% the diameter of an AM particle for CB-AM interaction) and replaced by a force that decreases with decreasing separation distance and changes into a strong repulsive force when overlapping occurs. The form of this force was determined so that two approaching particles could come into contact with negligible overlapping and vibration, which we observed did not affect the configuration of the particle cluster.

Key factors and aggregates characterization.—We employed a design of experiment to study the effect of key factors (temperature, particle size, and mass ratio) on the aggregate geometry. We assigned the temperature to three levels: 298, 308 and 328 K, the size of the AM particles from 0.5 to 1.0 μm, and CB/AM mass ratio from 4%:92% to 8%:88%. We performed five simulation runs for each combination and characterized the resulting aggregates in terms of the number of CB particles connected to AM particle clusters. In all simulation cases, the AM particle number and solid volume fraction were constant.

We selected the parameters for the following reasons: (1) the temperature has a high influence on the magnitude of Brownian forces, which helps the particles overcome local minima and achieve an energetically favorable (stable) state; on the other hand, high temperature can also cause bonds between particles to break due to large random motion; (2) the size of AM particles has a high influence on the performance of batteries (optimizing for energy or power), and particle size also affects the magnitude of forces that they exert on surrounding particles; (3) The CB is an additive that improves conductivity, it is desirable to optimize the mass ratio of CB and AM to get more conductivity with minimum added mass.

The aggregates generated using the above-mentioned simulation algorithm were characterized in order to identify the key parameters that determine the final structure geometry.

In our simulation, we recorded whether each pair of particles was connected. Using this information, we built a cluster list in which the connected particles were grouped in the same cluster. In order to improve the conductivity of the electrode material, the connection between CB particles and AM particle clusters is an important parameter. At a given CB content, it is reasonable to assume that the more CB particles connect to AM particle clusters, the bigger contribution they make to the improvement of conductivity of the cathode system. Therefore we characterize the aggregated system by the percentage of CB particles connected to the AM particles, using the cluster list we found.

Results

Final configuration.—A representation of the final configuration obtained through Brownian dynamic simulation is shown in Fig. 3. The larger blue spheres represent AM particles while the red smaller

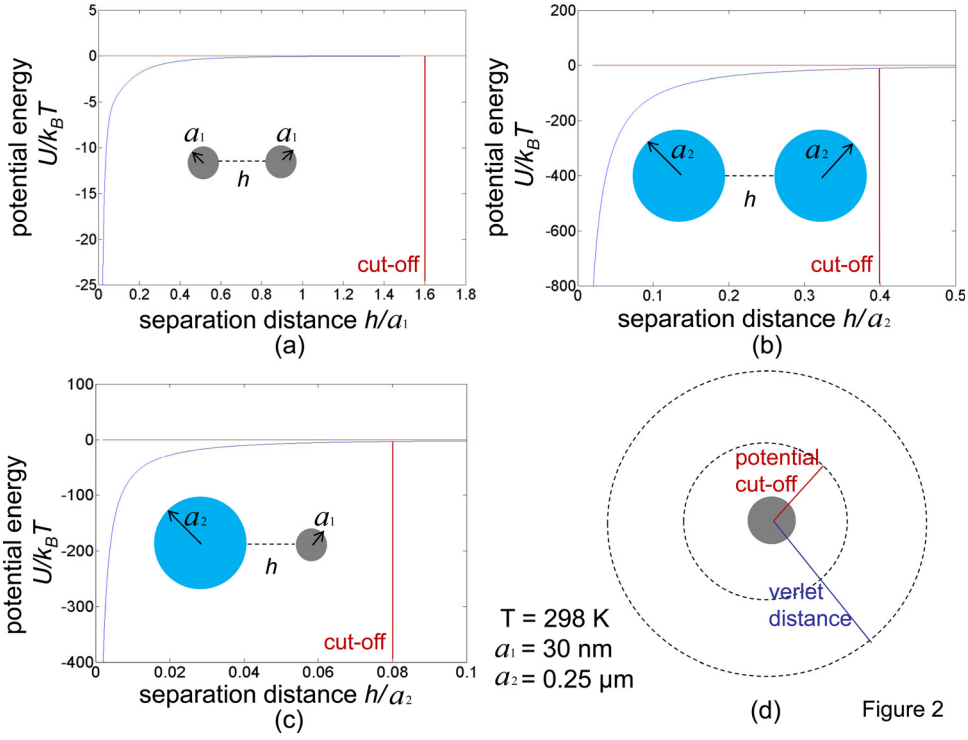

Figure 2. (Color online) Schematics of potential energy drop off and interaction distances. (a) CB-CB; (b) MnO_x-MnO_x; (c) CB-MnO_x; (d) potential cut-off and Verlet distance.

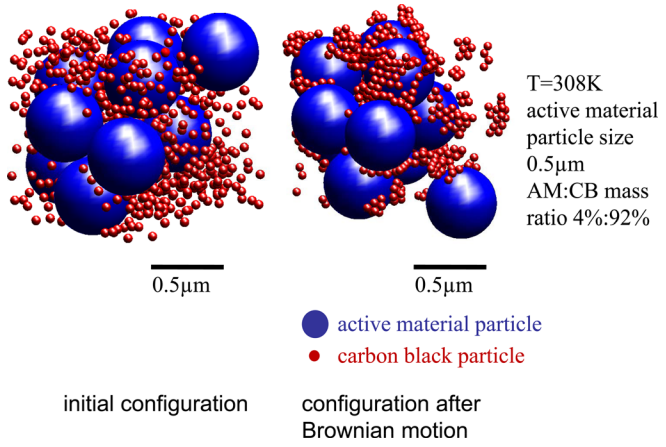

Figure 3. (Color online) Aggregated structure after Brownian dynamic simulation.

spheres represent CB particles. AM particles occupy the most volume within the domain due to their larger size and form a percolated network. The CB particles are connected to AM particles by means of attractive forces. Also, relatively short-ranged attractive forces between CB particles form local clusters among them. These clusters are attracted to the AM particle network, improving conductivity of the electrode. Fundamentally, the configurations of the system are determined by the combination of interactions due to van der Waals force, electrostatic force, and random forces. Temperature also plays an important role in determining the system structure. Brownian motion, which is temperature dependent, can shake the CB and AM particles to prevent the system from being trapped into a local minimum.

Effect of temperature.—For AM particles with a diameter of 0.5 and 1.0 μm, and for systems with a CB/AM mass ratio of 4%:92% and 8%:88%, the percentage of CB particles (out of a total of 629, 1315 or 5032 CB particles being simulated) that connected to the cluster of aggregated AM is plotted against different temperature levels in Fig. 4. Our simulation results show that when temperature increases, the percentage of CB particles connected to AM clusters increases for cases with AM particles 1 μm in diameter (Fig. 4b). However this percentage decreases for AM particles with a diameter of 0.5 μm (Figs. 4a and 4c). The P-value for the null-hypothesis (that there no difference in mean for samples from cases with different temperature levels) is small (0.0085 and 1.34e-7) for the two cases with a CB/AM mass ratio 4%:92% (Figs. 4a and 4b), indicating a significant correlation between temperature and CB connection. However, for cases with a CB/AM mass ratio of 8%:88% (Fig. 4c), the P-value is found to be larger (0.073), indicating a weaker correlation. Our explanation for the cases with AM particle size 1.0 μm is that the increase in temperature increases the Brownian motion of particles and enhances their ability to overcome the energy barrier and minimize potential. However, for the cases with an AM particle size 0.5 μm, due to the weaker attraction forces between AM particles and CB particles, the Brownian motion becomes more significant with increased temperature, causing easier bond separation.

Effect of AM particle size.—When the particle size increase from 0.5 to 1.0 μm and the mass ratio of CB and AM were kept constant (4%:92%), the percentage of CB particles connected to AM particles (averaged across all temperature values) increased from 25.0% to 43.2%. The larger AM particle size increases the attraction force to CB particles, and thus increases the percentage of CB particles that are connected to the AM cluster.

Effect of CB/AM mass ratio.—When the AM particle size is kept at 0.5 μm and the mass ratio of CB and AM is increased from 4%:92% to 8%:88%, the percentage of CB connection (averaged

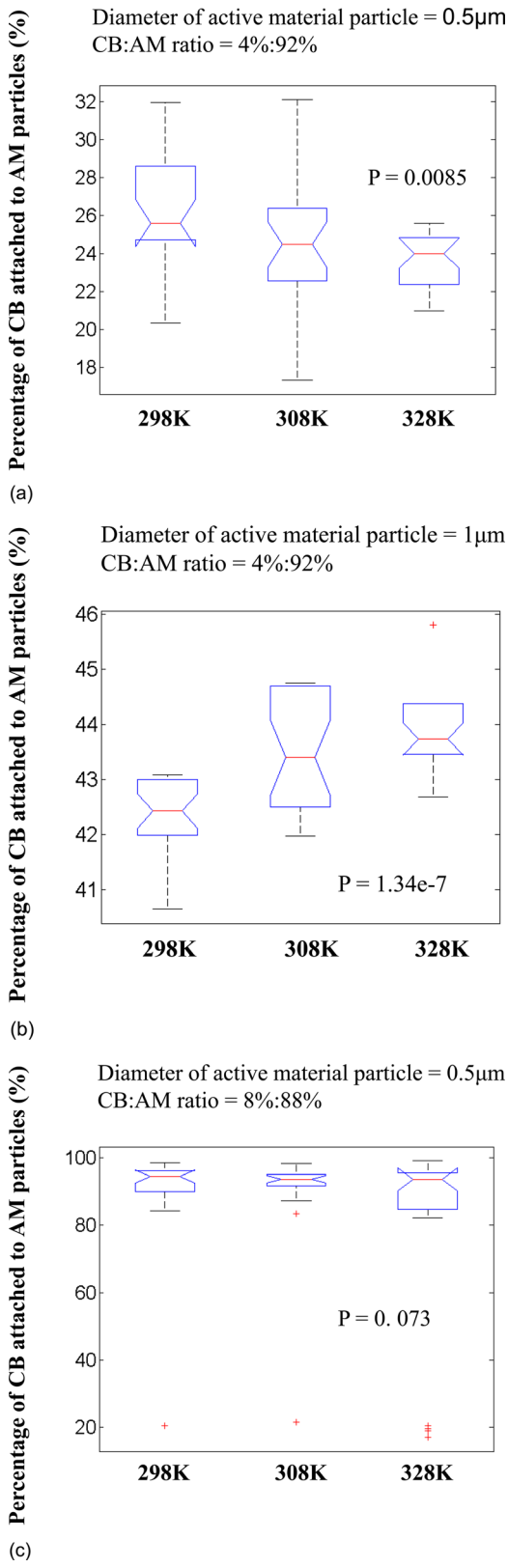

Figure 4. (Color online) Number of CB connected to AM cluster plotted against temperature, with different AM particle size and CB/AM ratios.

across all temperature values) increases from 25.0% to 86.4%. The larger CB mass ratio increases the probability for CB particles to interact among themselves and interact with AM particles, thus improving the conductive network by increasing the CB connection rate.

Conclusions

Brownian dynamic simulation was performed on a binary system (CB and AM spherical particles) with a solid volume fraction of 50%. The final configuration from the simulation shows that all AM particles are aggregated into a single cluster and percolate the simulation domain. Local aggregates of CB particles are observed. CB particles are also observed to connect to the percolated AM clusters. In a battery cathode, it is desirable for a large number of CB particles to connect to AM particles to form pathways for electrons to flow, which increases the conductivity of the electrode.

Our simulation results show that larger AM particle size and higher CB/AM mass ratio each contributes positively to the percentage of CB particles that connect to the percolated AM cluster. Larger AM particle size leads to larger attraction forces binding the CB particles around the AM cluster, thus increasing the percentage of CB attachment. Higher CB/AM mass ratio means a larger CB particle number for a given number of AM particles, so that the CB particles will have a higher probability of interacting with each other and with AM particles, leading to a higher percentage of attachment.

However, the percentage of CB attachment increases with increasing temperature for AM particles with a diameter of 1 μm but decreases for AM particles with a diameter of 0.5 μm. Increasing temperature leads to increasing Brownian motion. When AM particles are larger, this Brownian motion enables CB particles to overcome the energy barrier and to minimize potential. However the attraction forces between AM particles and CB particles will be large enough to reduce the probability of debond due to Brownian motion. The end result is an increasing percentage of CB particles connecting to the AM cluster. However, in the cases where AM particles are small, the attraction forces are weaker. Higher Brownian motion caused by higher temperature can disturb the connection between particles leading to a decrease in the percentage of CB attachment. In addition, Brownian motion effect is more significant for system with smaller particle size, which also contributes to the decrease in the CB attachment for smaller AM particles.

In this work, the cathode aggregation process of Li-ion batteries is simulated to find the relative position of different particles, the first step in providing insight into optimizing battery cathodes. We have demonstrated the trend between CB connection percentage and particle size, mass ratio and temperature. Further simulation of solvent (NMP) evaporation and the formation of PVDF solid phase following the aggregation process will enable us to determine the electrical conductivity as well as other properties of the fabricated cathode. Further simulations in the future could map in detail the parameters discussed in this work and find the optimum conditions that maximize conductivity with minimal added mass.

Acknowledgments

This effort was supported by the Department of Energy, with additional sponsorship by the General Motors/University of Michigan Advanced Battery Coalition for Drivetrains. The authors appreciate the support from our sponsors.

List of Symbols

AM	active material
CB	carbon black
NMP	*N*-methylpyrrolidone
PVDF	polyvinylidene difluoride

References

1. S. Y. Chung, J. T. Bloking, and Y. M. Chiang, *Nature Mater.*, **1**, 123 (2002).
2. G. Liu, H. Zheng, A. S. Simens, A. M. Minor, X. Song, and V. S. Battaglia, *J. Electrochem. Soc.*, **154**, A1129 (2007).
3. X. Zhang, P. N. Ross, Jr., R. Kostecki, F. Kong, S. Sloop, J. B. Kerr, K. Striebel, E. J. Cairns, and F. McLarnon, *J. Electrochem. Soc.*, **148**, A463 (2001).
4. C. P. Fonseca, E. M. J. A. Pallone, and S. Neves, *Solid State Sciences*, **6**, 1353 (2004).
5. Y.-H. Chen, C.-W. Wang, X. Zhang, and A. M. Sastry, *J. Power Sources*, **195**, 2851 (2010).
6. M. Manickam and M. Takata, *Electrochim. Acta*, **48**, 957 (2003).
7. S. Mandal, J. M. Amarilla, J. Ibanez, and J. M. Rojo, *J. Electrochem. Soc.*, **148**, A24 (2001).
8. E. Ligneel, B. Lestriez, A. Hudhomme, and D. Guyomard, *J. Eur. Ceram. Soc.*, **29**, 925 (2009).
9. D. Guy, B. Lestriez, R. Bouchet, and D. Guyomard, *J. Electrochem. Soc.*, **153**, A679 (2006).
10. E. Ligneel, B. Lestriez, and D. Guyomard, *J. Power Sources*, **174**, 716 (2007).
11. G. Liu, H. Zheng, A. S. Simens, A. M. Minor, X. Song, and V. S. Battaglia, *J. Electrochem. Soc.*, **154**, A1129 (2007).
12. G. Liu, H. Zheng, S. Kim, Y. Deng, A. M. Minor, X. Song, and V. S. Battaglia, *J. Electrochem. Soc.*, **155**, A887 (2008).
13. M.-R. Lim, Wan-Il. Cho, and K.-B. Kim, *J. Power Sources*, **92**, 168 (2001).
14. D. Wang, X. Wu, Z. Wang, and L. Chen, *J. Power Sources*, **140**, 125 (2005).
15. H. Wang, Young-Il. Jang, B. Huang, D. R. Sadoway, and Y.-M. Chiang, *J. Electrochem. Soc.*, **146**, 473 (1999).
16. G. Liu, H. Zheng, S. Kim, Y. Deng, A. M. Minor, X. Song, and V. S. Battaglia, *J. Electrochem. Soc.*, **155**, A887 (2008).
17. M. Hutter, *J. Colloid Interface Sci.*, **231**, 337 (2000).
18. I. Schenker, F. T. Filser, T. Aste, and L. J. Gauckler, *J. Eur. Ceram. Soc.*, **28**, 1443 (2008).
19. M. Hecht and J. Harting, *Int. J. Mod. Phys. C*, **18**, 501 (2007).
20. M. Cerbelaud, A. Videcoq, P. Ablard, C. Pagnoux, F. Rossignol, and R. Ferrando, *Langmuir*, **24**, 3001 (2008).
21. M. Elimelech, J. Gregory, X. Jia, and R. A. Williams, *Particle Deposition and Aggregation: Measurement, Modeling and Simulation*, Butterworth-Heinemann, Oxford, England (1995).
22. R. R. Dagastine, D. C. Prieve, and L. R. White, *J. Colloid Interface Sci.*, **249**, 78 (2002).
23. D. M. Keman and W. J. Blau, *EPL*, **83**, 66009 (2008).
24. Y. K. Cho, R. Wartena, S. M. Tobias, and Y.-M. Chiang, *Adv. Funct. Mater.*, **17**, 379 (2007).
25. C. Na and S. T. Martin, *Environ. Sci. Technol.*, **43**, 4967 (2009).
26. P. C. Hiemenz and R. Rajagopalam, *Principle of Colloid and Surface Chemistry*, 3rd ed., Dekker. New York, 1997.
27. ASTM Standard D, Zeta Potential of Colloids in Water and Waste Water, American Society for Testing and Materials, ASTM Standard D, 4187-82. 1985.
28. R. P. Jaiswal, G. Kumar, C. M. Kilroy, and S. I. Beaudoin, *Langmuir*, **25**, 10612 (2009).
29. A. Basch, R. Horn, and J. O. Besenhard, *Colloids Surf., A*, **253**, 155 (2005).
30. D. W. Fuerstenau and J. Shibata, *Int. J. Min. Process.*, **57**, 205 (1999).
31. T. Masuda, Y. Matsuki, and T. Shimoda, *J. Colloid Interface Sci.*, **340**, 298 (2009).
32. M. P. Allen and D. J. Tildesley, *Computer Simulation of Liquids*, Clarendon, Oxford (1987).